HEAD-MOTION COMPENSATION DURING RECONSTRUCTION FROM LIST-MODE PET DATA

W. Deckers*, J. Verhaeghe*, J. De Beenhouwer*, Y. D'Asseler* and I. Lemahieu*

* Ghent University/ELIS-MEDISIP, Ghent, Belgium

jeroen.verhaeghe@ugent.be

Abstract: Patient motion during PET imaging is responsible for resolution loss, this problem is related to the time consuming scan. We have implemented a list-mode based motion compensation scheme that deals with the six degrees of freedom of a rigid body patient movement. During an acquisition several millions of coincident events are detected and patient motion is tracked. The compensation technique corrects the detected events for the measured motion and the reconstruction follows a standard iterative MLEM reconstruction algorithm using a for motion corrected sensitivity profile. We have tested our implementation using a software and hardware Hoffman brain phantom. The algorithm could compensate for the simulated motion and the resulting images showed less blurring.

Introduction

During a positron emission tomography (PET) scan subjects are asked to lie still for several minutes. Neurological brain scans can even take several tens of minutes. PET scans are therefore prone to motion artifacts. With the advent of high spatial resolution scanners, patient motion becomes an increasingly important image degrading effect. Even due to a small involuntary movements, the reconstructed image can be severely degraded. The use of a head restraint system cannot fully prevent motion [1–3] and introduces some physiological stress. In the worst case scenario the motion artifacts are so bad that a new scan has to be performed. Motion compensation methods could prevent such resource expensive practice and could greatly enhance the image quality. Furthermore some of the most interesting patients are now excluded from PET studies (e.g. Parkinson and Gilles de la Tourette patients). Several methods have been extensively studied.

Image based techniques [2–5] divide the scan interval into smaller time-frames. The idea is that less motion occurs during such a shorter frame and severely motion affected frames can be discarded. The individual frames are then reconstructed, aligned and stacked. The main disadvantages of such methods is that they fail to correct for motion during a frame and the computational cost related to the fully 3D registration [6]. These problems could be solved by using a motion tracking device triggering the frames. However in the case of constantly moving patients such a method will lead to a large amount of low-count frames and poorly reconstructed images.

Projection based techniques [4, 7–9] try to use the same principle of multiple acquisition frames together with the use of a motion tracking system. But rather than reconstructing the individual frames separately a motion corrected projection data set is created whether the data is in sinogram format or in list-mode format. The list-mode format stores all the events detected in coincidence in a list. The events are specified by their Line-Of-Response (LOR) and detection time. Whereas for the sinogram format the tracking device should trigger the frames; the list-mode format requires a timing synchronization between the tracking devices and the list-mode acquisition module. The correction technique produces correction factors and transforms the LOR in which the event was detected into the LOR in which the event would have been detected had the object not moved. We have implemented such a projection based technique based on list-mode data.

Finally different techniques for rigid body motion tracking are described in literature [4,5,7,9]. They use passive (reflective) or active (emissive) markers fixated on the examined subject. The tracking device detects the motion by measuring the six degrees of freedom: three translations and three rotations. Typical positioning resolution range from 0.02 to 0.35 mm.

Theory

We used the iterative maximum likelihood - expectation maximization algorithm (MLEM) [10] for the reconstruction. For list-mode date the update formula reads [11]:

$$\lambda_i^{m+1} = \frac{\lambda_i^m}{TS_i} \sum_{events} \frac{p_{ij_e}}{\bar{y}_{j_e}^m}, \tag{1}$$

where λ_i^m is the reconstructed activity after m iterations at voxel i, T is the scan duration $S_i = \sum_j^J p_{ij}$ is the probability that an event originating from voxel i is detected by one of the scanners' J coincidence bins j. The sum is over all detected events and the coincidence bin at which the e-th was detected is denoted by j_e. p_{ij} is the probability that an event originating from voxel i is detected by coincidence bin j. The forward projection of the activity at iteration m is given by:

$$\bar{y}_j^m = \sum_i^I p_{ij} \lambda_i^m. \tag{2}$$

ISSN: 1727-1983

The image at $m = \infty$ is the maximum likelihood estimate. We can separate the probability p_{ij} into a geometrical component g_{ij} and LOR specific weight w_j . The w_j is in turn the combination of a detector pair specific normalization factor n_j and an attenuation factor a_j. We thus have $p_{ij} = g_{ij} n_j a_j$. For computational efficiency we prefer a LOR driven attenuation correction which precorrects the data for attenuation [12] and we have:

$$\lambda_i^{m+1} = \frac{\lambda_i^m}{TS'_i} \sum_{events} g_{ij_e} \frac{1/a_{j_e}}{\sum_i^I g_{ij_e} \lambda_i^m}, \qquad (3)$$

with $S'_i = \sum_j^J g_{ij} n_j$.
For the reconstruction we will attach the reconstruction grid $(1,\ldots,i,\ldots,I)$ to the studied object. Let us now introduce a patient movement. In image space this will have no effect on the indexing because the grid moves together with the object. In projection space a mapping M_t which maps an event detected at time t and coincidence bin j_t to the corresponding coincidence bin j_0 at which the event would have been detected at time $t = 0$. If there had been no motion during the interval $[0,t]$ then M_t is the identity operator. The operator can be constructed based on the motion tracking data and based on the geometry of the scanner. The grid and operator are illustrated in Fig.1. In Fig.1 (a) the reference system is depicted at time

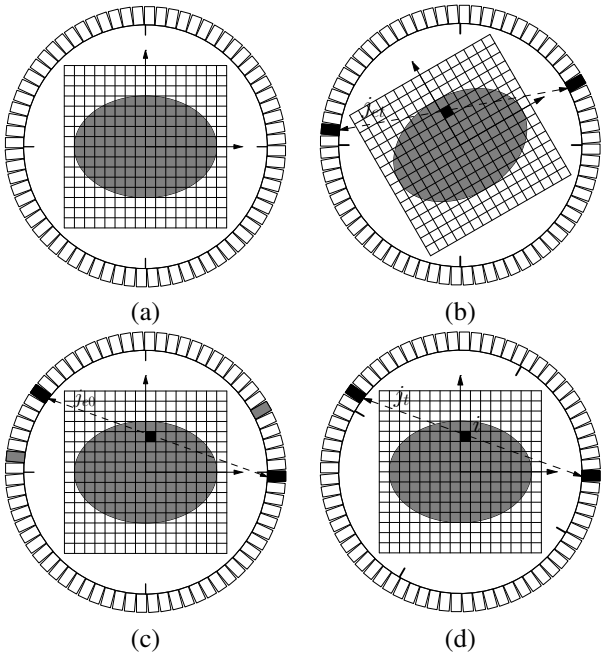

Figure 1: The scanner geometry: (a) the initial set-up at time t_o. In (b) an event is detected in bin j at time t: j_{et}. The compensation transforms the LOR to j_{e0} the LOR that would have detected the coincidence event in the absence of motion (c). For the calculation of the sensitivity factor of voxel i we need to transform the scanner following M_t^{-1}.

$t_0 = 0$, (b) shows a coincidence detection in bin j_{et} at time t. Rather than re-sampling the sensitivity pattern following the new grid (Fig.1 (b)) we transform the LOR into the LOR in which the detection would have been detected in the absence of motion (Fig.1 (c)), i.e. $j_{e0} = M_t(j_{et})$. The path through the grid and the object is the same for j_{et} and j_{e0} as can been seen in Fig.1(b,c). The crystals detecting the photons have changed however (Fig.1 (c) black and gray crystals). Now for the motion corrected MLEM algorithm the update formula becomes [8]

$$\lambda_i^{m+1} = \frac{\lambda_i^m}{\bar{S}_i} \sum_{events} g_{ij_{e0}} \frac{1/a_{j_{e0}}}{\sum_i^I g_{ij_{e0}} \lambda_i^m}, \qquad (4)$$

where we use the transformed LOR j_{e0} and the sensitivity term TS'_i in (3) is replaced by

$$\bar{S}_i = \sum_j^J g_{ij} \int_0^T n_{j_t} dt \qquad (5)$$

which requires the normalization factor n_{j_t} at bin j_t with $M_t(j_t) = j$. It just seems as if the detector is moving following M_t^{-1} (Fig.1 (d)). It is of course possible that events emitted under a given angle with respect to the moving grid detected at $t = 0$ in bin j_0 will not cross the detector at time t due to the motion. At this point one could think of introducing a virtual detector bin j_t with $n_{j_t} = 0$.

Methods

We have implemented a motion compensation method for list-mode format following (4). We ran a parallelized version of our previously developed MLEM algorithm [13]. The program makes use of LAM/MPI [14] a freely available, open source implementation of the Message Passing Interface (MPI). During one iteration the program divides the coincidence events over the available worker nodes which are then processed (projection and back-projection) by the nodes. After processing all the events the correction factors are collected at one node and multiplied with the old activity estimate to form the new estimate which is then broadcasted to all the nodes.
The geometric factors g_{ij} are calculated using the simple line-length Siddon algorithm [15]. For this purpose we can describe a LOR by two points defining the line, which makes it easy to calculate the mapping function M_t from the motion tracking data. In this case M_t can be described by a rotation and a translation that can readily be applied to the points describing the LOR.
The algorithm proceeds as follows. The data from the PET scanner and the motion tracking device are read. We step through the list-mode data and the arrival times t_e determine the set of motion tracking parameters used to build up the mapping M_{t_e}. The mapping is then applied to the two points determining j_{et} to produce the new points determining the new line corresponding with j_{e0}. The corrected LOR is then written to the motion corrected list-mode file. Secondly the sensitivity map should be calculated and in particular $\int_0^T n_{j_t} dt$. The calculation steps through the tracking data and the

ISSN: 1727-1983

tracking parameters determine now the inverse mapping M_t^{-1} which is then applied to all original j's to form j_t and the corresponding n_{j_t} can be found in the Look Up Table (LUT) or equals zero if the transformed 'virtual' LOR does not intersect the scanner.
We have evaluated our method using both software phantoms and hardware data. The simulator was a geometrical perfect simulator and no scatter or random events were simulated. All emitted photons were detected in a perfect ring detector and were recorded in list-mode format. The voxelized source distribution could be translated and rotated and these parameters were used as the simulated motion tracking data.

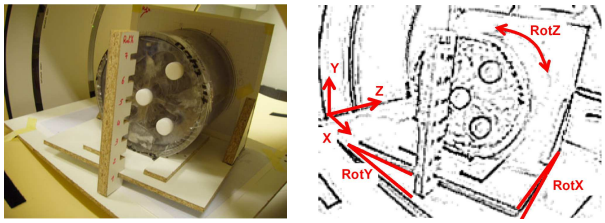

(a) (b)

Figure 2: The mount designed for controlled motion and its degrees of freedom.

The measurements were performed on a Philips Gemini PET/CT scanner at the University Hospital Ghent (UZ Gent). No tracking device was available. To simulate motion in a controlled way we have developed a mount (Fig.2). The phantom could be rotated and shifted manually and the motion could be marked on the mount for later use as simulated tracking data. A Hoffman brain phantom [16] filled with $1.1mCi$ of F^{18}-FDG was used. The motion parameters are summarized in Table 1.

Table 1: Simulated motion for the Hoffman brain phantom on the Phillips Gemini.

Δt (min)	t_x (mm)	t_y (mm)	t_z (mm)	$rotX$ $(^\circ)$	$rotY$ $(^\circ)$	$rotZ$ $(^\circ)$
2						
2			11.5			
2	13.0		25.0	12.0	9.5	
2						18.9
5		31.0				
5	16.0		−68.5	−7.0	23.0	

Results

The software Hoffman phantom data was reconstructed both with and without motion compensation. The motion algorithm performed well and resulted in better images. Typical transverse and coronal slices are depicted in Fig.3. In this set-up the phantom underwent a rotation of 5° about the x-axis, a rotation of 15° about the z-axis and a translation of $5mm$ in the z-direction. The images with

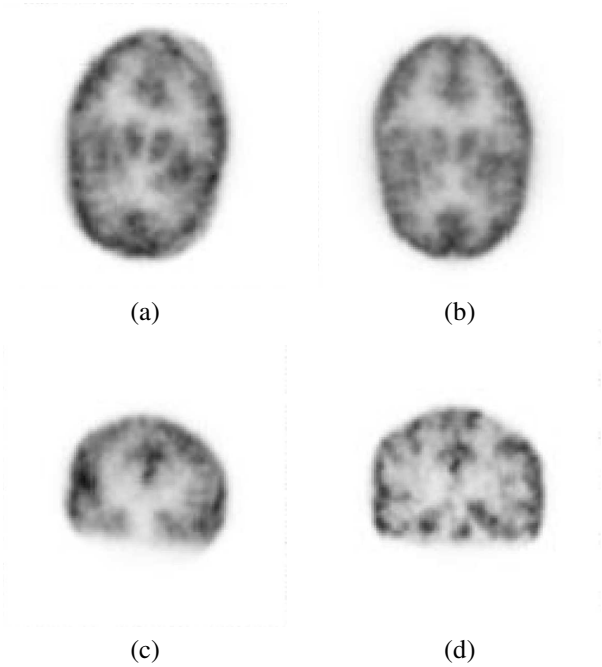

(a) (b)

(c) (d)

Figure 3: Transverse and coronal slices reconstruction of the software Hoffman phantom without motion compensation (a) and (c) compared to reconstructions with motion compensation (b) and (d).

motion compensation show more detail as compaired to the images without motion correction which are blurred due to the motion. This is especially obvious for the gyri and sulci.

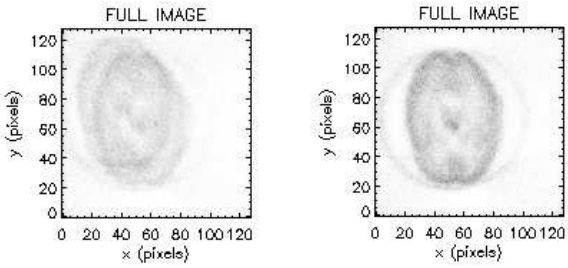

(a) (b)

Figure 4: Reconstruction of the (hardware) Hoffman brain phantom without (a) and with (b) motion compensation

Finally example reconstructions for the Phillips Gemini data are presented in Fig.4. The data used for the reconstruction is only the part of the acquisition corresponding to rows 4 and 5 of Table 1. So the only relative movement is a translation of $31mm$ in the y-direction. Note that due to the earlier movements the y-direction of the translation does not correspond with the y-direction of the image in Fig.4. Again we can see an important improvement in the reconstruction using motion correction (Fig.4(a)) compared to the reconstruction without motion correction (Fig.4(b)).

ISSN: 1727-1983

Discussion and conclusion

Patient movement during a positron emission tomography scan is an important image degrading factor. Motion correction techniques could reduce the blur introduced by the patient movement.
We have implemented a list-mode based motion compensation scheme spatially transforming the lines of response and temporally averaging the sensitivity factors. This method is particularly suited for rigid objects such as the human brain.
The first encouraging results of the method are presented here. A reconstruction using the motion correction technique visually resulted in better images.
We plan to perform further experiments using a real motion tracking system which could also allow us to perform phantom studies with continuous displacements and human studies.

Acknowledgment

This work was supported in part by the "Bijzonder Onderzoeksfonds" (BOF) of the Ghent University.

References

[1] RUTTIMANN, U. E. , ANDREASON, P. J., and RIO, D. Head motion during positron emission tomography is it significant. *Psychiatry Research-Neuroimaging*, 61(1):43–51, 1995.

[2] GREEN, M. V., SEIDEL, J., STEIN, S. D., TEDDER, T. E., KEMPNER, K. M., KERTZMAN, C., and ZEFFIRO, T. A. Head movement in normal subjects during simulated PET brain imaging with and without head restraint. *Journal of Nuclear Medicine*, 35(9):1538–1546, 1994.

[3] HUTTON, B. F., KYME, A. Z., LAU, Y. H., SKERRETT, D. W., and FULTON, R. R. A hybrid 3-D reconstruction/registration algorithm for correction of head motion in emission tomography. *IEEE Transactions on Nuclear Science*, 49(1):188–194, 2002.

[4] MENKE, M. , ATKINS, M. S., and BUCKLEY, K. R. Compensation methods for head motion detected during PET imaging. *IEEE Transactions on Nuclear Science*, 43(1):310–317, 1996.

[5] PICARD, Y. and THOMPSON, C. J. Motion correction of PET images using multiple acquisition frames. *IEEE Transactions on Medical Imaging*, 16(2):137–144, 1997.

[6] STUDHOLME, C., HILL, D. L. G., and HAWKES, D. J. An overlap invariant entropy measure of 3D medical image alignment. *Pattern Recognition*, 32(1):71–86, 1999.

[7] BLOOMFIELD, P. M., SPINKS, T. J., REED, J., SCHNORR, L., WESTRIP, A. M., LIVIERATOS, L., FULTON, R., and JONES, T. The design and implementation of a motion correction scheme for neurological PET. *Physics In Medicine and Biology*, 48(8):959–978, 2003.

[8] RAHMIM, A., BLOOMFIELD, P., HOULE, S., LENOX, M., MICHEL, C., BUCKLEY, K. R., RUTH, T. J., and SOSSI, V. Motion compensation in histogram-mode and list-mode EM reconstructions: Beyond the event-driven approach. *IEEE Transactions on Nuclear Science*, 51(5):2588–2596, 2004.

[9] BUHLER, P., JUST, U., WILL, E., KOTZERKE, J., and VAN DEN HOFF, J. An accurate method for correction of head movement in PET. *IEEE Transactions on Medical Imaging*, 23(9):1176–1185, 2004.

[10] SHEPP, L. A., VARDI, Y., RA, J. B., HILAL, S. K., and CHO, Z. H. Maximum-likelihood PET with real data. *IEEE Transactions on Nuclear Science*, 31(2):910–913, 1984.

[11] BARRETT, H. H., WHITE, T., and PARRA, L. C. List-mode likelihood. *Journal of the Optical Society of America A-Optics Image Science and Vision*, 14(11):2914–2923, 1997.

[12] R. AND FALIKMAN, D. LEVKOVITZ, ZIBULEVSKY, M., BEN-TAL, A., and NEMIROVSKI, A. The design and implementation of COSEM, an iterative algorithm for fully 3-D listmode data. *IEEE Transactions On Medical Imaging*, 20(7):633–642, 2001.

[13] VERHAEGHE, J., D'ASSELER, Y., DE WINTER, O. , STAELENS, S., VAN DE WALLE, R. , and LEMAHIEU, I. Five dimensional reconstruction on tensor product splines in cardiac PET. In *Proceedings of the 8th International Meeting on Fully Three-dimensional Image Reconstruction in Radiology and Nuclear Medicine*, pages 167–171, Salt Lake City, 7 2005.

[14] LAM/MPI. `http://www.lam-mpi.org/`.

[15] SIDDON, R. L. Fast calculation of the exact radiological path for a 3-dimensional CT array. *Medical Physics*, 12(2):252–255, 1985.

[16] HOFFMAN, E. J., CUTLER, P. D., DIGBY, W. M., and MAZZIOTTA, J. C. 3-D phantom to simulate cerebral blood-flow and metabolic images for PET. *IEEE Transactions on Nuclear Science*, 37(2):616–620, 1990.

ISSN: 1727-1983